Electronic Supporting Information (ESI)

A core-shell structured biphasic microneedle system as elite squad for combating melanoma with "three-in-one" therapeutic power

*Qiling Jin[#a], Ying Wang[#a], Wenwen Lei[a], Shuyao Zhou[a], Tingting Zhang[a], Keqiang Lu[d], Lingzhi Zhao[*d], Wenying Zhong[*abc], Keming Xu[*ab]*

[a]Department of Chemistry, China Pharmaceutical University, Nanjing 210009, China.

[b]Key Laboratory of Biomedical Functional Materials, China Pharmaceutical University, Nanjing 210009, China.

[c]Key Laboratory of Drug Quality Control and Pharmacovigilance, China Pharmaceutical University, Nanjing 210009, China.

[d]State Key Laboratory of Natural Medicine, The School of Basic Medical Sciences and Clinical Pharmacy, China Pharmaceutical University, Nanjing 211198, China.

Address: China Pharmaceutical University, 639 Longmian Avenue, Jiangning District, Nanjing, Jiangsu, P. R. China.

[#] Equal contribution.

* kmxu@cpu.edu.cn; wyzhong@cpu.edu; zlz@cpu.edu.cn

Table of contents

Figure S11. (A) The images of PCHAT-Ce6@NPs-MNs after application of a 30 N mechanical force. (i) Ce6@NPs-MNs, (ii) PCHAT-Low-Ce6@NPs-MNs, (iii) PCHAT-Medium-Ce6@NPs-MNs and (iv) PCHAT-High-Ce6@NPs-MNs. (B) The percentage of height of four MNs.

Figure S12. Number of holes created by Ce6@NPs-MNs and various PCHAT-Ce6@NPs-MNs on each layer of parafilm.

Figure S13. The puncture force-displacement curves of various microneedles on porcine skin.

Figure S14. (A) Optical microscopy images of four MNs after insertion into agarose gel at different time points. (i) Ce6@NPs-MNs, (ii) PCHAT-Low-Ce6@NPs-MNs, (iii) PCHAT-Medium-Ce6@NPs-MNs and (iv) PCHAT-High-Ce6@NPs-MNs. (B) Optical microscopy images of four MNs after insertion into porcine skin after 5 min. (i) Ce6@NPs-MNs, (ii) PCHAT-Low-Ce6@NPs-MNs, (iii) PCHAT-Medium-Ce6@NPs-MNs and (iv) PCHAT-High-Ce6@NPs-MNs. Scale bar: 200 μm.

Figure S15. Percentages of drug release from Ce6@NPs-MNs, PCHAT-Low-Ce6@NPs-MNs, PCHAT-Medium-Ce6@NPs-MNs and PCHAT-High-Ce6@NPs-MNs at different time points.

Figure S16. (A) CLSM images of A375 cells receiving 2 h pretreatment of 30 μM CPZ, 1 μg/mL Filipin III, EIPA 50 μM or CytD 20 μM prior to the addition of Ce6@NPs + HA. (B) The mean fluorescence intensity of red signals in the cells images of (A).

Figure S17. Changes of body weight in A375-xenografted mice after various treatments.

Figure S18. Representative H & E-stained images of major organ tissues (heart, liver, spleen, lung, kidney) from mice after different treatments. Groups: (i) PBS; (ii) PCHAT-Ce6@NPs-MNs + Laser. Scale bar: 100 μm.

Figure S19. Histological analyses of skin tissue at the laser sites. (A) H & E staining of skin tissue before laser irradiation. (B) H&E staining of skin tissue after 5 min of laser irradiation. Scale bar, 500 μm.

Figure S20. Histological analysis of skin tissue at the site of microneedle application. (A) H & E staining of skin tissue from the control group. (B) H & E staining of skin tissue 15 days after microneedle application. Scale bar: 500 μm.

Figure S21. Quantitative analysis of serum ALT (A) and AST (B) levels after 15 days of different treatments. ns: no significance.

Figure S22. Quantifications of GSH (A), GPx (B), and MDA (C) levels in tumor tissues after various treatment.

Figure S23. (A) Representative H & E-stained images of tumor tissue sections after various treatments. (B) Representative TUNEL-stained images of tumor tissue sections, with arrows indicating apoptotic cells. Groups: (ii) PCHAT-MNs; (iii) Laser; (iv) PCHAT-Ce6@NPs-MNs. Scale bar: 100 μm.

Figure S24. Percentages of apoptotic cells in tumor tissues after various treatment.

Experimental

Stability of RhB in PMMA/HA-MNs under different environmental conditions

Different groups of microneedle patches were placed under various temperature and humidity environments (25 °C, 60%; 25 °C, 30%; 25 °C, 15%; 37 °C, 30%) for one week. After that, the tips of the microneedles from each group were scraped off, and dissolved in PBS. The fluorescence intensity of RhB in the tips was then measured using fluorescence spectrophotometry (Excitation: 555 nm; Emission: 570-650 nm).

Synthesis and characterization of tyramine-modified hyaluronic acid (HAT)

Tyramine (Tyr) was covalently attached to the side chains of hyaluronic acid (HA) via an EDC/NHS coupling reaction. HA (3 g, 74K Da, 2.6 mmol of repeating disaccharide units) was dissolved in 300 mL of ultrapure water under stirring. EDC·HCl (1644 mg, 8.58 mmol) and NHS (996 mg, 8.58 mmol) were then added to the solution to fully activate the carboxyl groups on the HA side chains. Subsequently, tyramine hydrochloride (1353 mg, 7.8 mmol) was added, and the pH was adjusted to approximately 4.7. The reaction was allowed to proceed overnight at room temperature. The next day, the solution was adjusted to pH 5.5 and transferred to a dialysis bag (MWCO = 3500 Da). Dialysis was performed sequentially with 0.1% NaCl for 2 days, followed by an ethanol/water mixture (1:3) and deionized water, each for 1 day. Finally, the product was freeze-dried to obtain a white flocculent HA-Tyr (HAT) substance.

The structure of HAT was confirmed using ultraviolet-visible spectroscopy (UV-vis) and proton nuclear magnetic resonance spectroscopy (^{1}H NMR, 400 MHz,

D_2O). The absorbance of the synthesized HAT was determined using UV-vis, and the degree of substitution of tyramine on the HA backbone was calculated.

Synthesis and characterizations of Ce6@NPs

Ce6@NPs were provided by Prof. Lingzhi Zhao team, and the synthesis method was detailed in the previous work.[1] The particle size and polydispersity index (PDI) of Ce6@NPs were recorded using a Nano ZS90 Malvern particle size analyzer. The morphology of NP/TMPyP was then characterized using transmission electron microscopy (JEM-2100F, Japan).

Investigation of different matrix materials

The effect of different matrices on the stability of Ce6@NPs was assessed using a Malvern zeta sizer. Ce6@NPs (40 μg/mL) were dispersed in 5 wt% solutions of chitosan (CS), polyvinyl alcohol (PVA), HA, respectively, and incubated in a constant temperature and humidity chamber at 25°C. The particle size was measured on day 0, 1, 3, 5, 7, 9, 11, and 13. The zeta potential of 1 mg/mL solutions of CS, PVA, HA, and Ce6@NPs at pH 7.4 was measured using a Malvern zeta sizer.

The effect of different matrices on the fluorescence intensity of Ce6@NPs was determined using fluorescence spectrophotometry. Ce6@NPs (30 μg/mL) were dispersed in 5 wt% solutions of CS, PVA, and HA, respectively. The excitation wavelength was set to 403 nm, the emission wavelength range to 600-750 nm, and the detection wavelength to 663 nm.

The 9,10-Anthracenediyl-bis(methylene)dimalonic acid (ABDA) was used as a ROS indicator to evaluate the effect of different matrices on the ability of Ce6@NPs

to generate ROS under near-infrared (NIR) irradiation. Ce6@NPs (10 μg/mL) were first dispersed in 5 wt% solutions of CS, PVA, and HA, respectively. ABDA solution (50 μg/mL) was then added and mixed thoroughly. After irradiation with a 650 nm laser at 0.5 W/cm² for different durations, the absorbance of the different solutions was measured using a UV-visible spectrophotometer.

Stability of Ce6 in PCHAT-Ce6@NPs-MNs under light irradiation

Ce6@NPs-MNs and PCHAT-Ce6@NPs-MNs were prepared and divided into dark and laser groups. The laser groups were irradiated with a 40-W blue light for 1 hour. Afterwards, the tips of the microneedles were scraped off, and the fluorescence intensity of Ce6 was measured (Excitation: 403 nm; Emission: 600-750 nm). The relative fluorescence intensity was then calculated by comparing the values of irridiation group with the corresponding dark group.

Biocompatibility evaluation of PCHAT-Ce6@NPs-MNs

Healthy C57BL/6 mice (Male) were used as the animal model and randomly divided into a control group and a PCHAT-Ce6@NPs-MNs treatment group. In the treatment group, the mice received administration of PCHAT-Ce6@NPs-MNs alongside laser irradiation (650 nm, 800 mW/cm², 5 min). Both groups were housed under identical conditions. After 14 days, skin tissues were collected for histological analysis using H&E staining. On the same day, the blood samples were collected for serum separation, followed by ALT and AST analysis using a commercial detection kit (Biosharp, Beijing Labgic Technology Company, China).

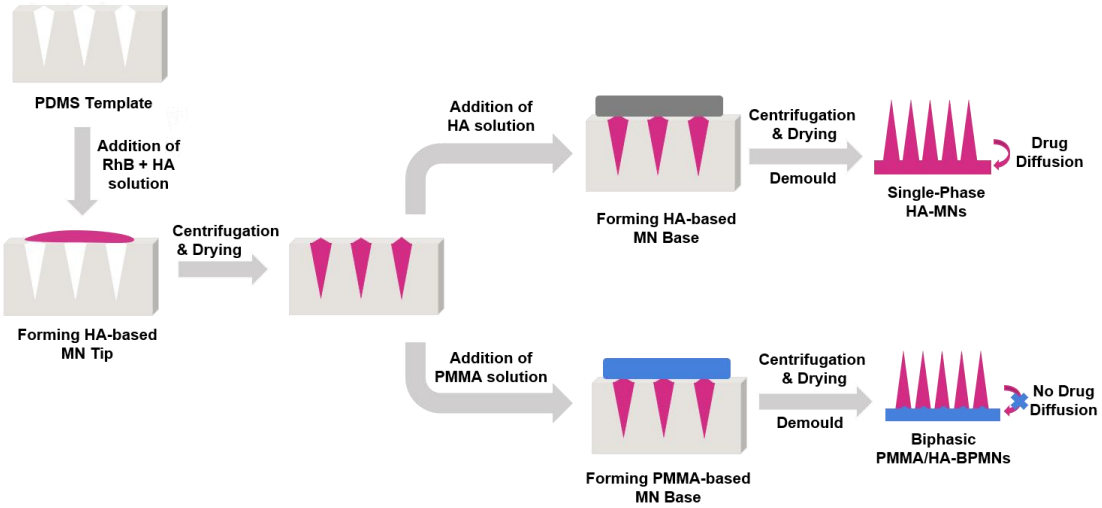

Scheme S1. Schematic illustration of the fabrication process for PMMA/HA-MNs and HA-MNs.

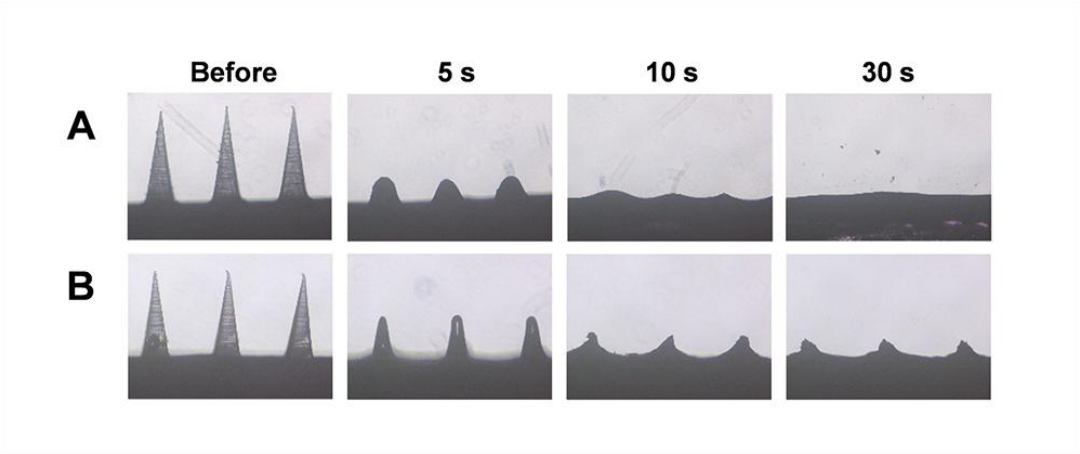

Figure S1. Optical microscopy images of PMMA/HA-MNs and HA-MNs after insertion into agarose gel at different time points. (A) HA-MNs, (B) PMMA/HA-MNs.

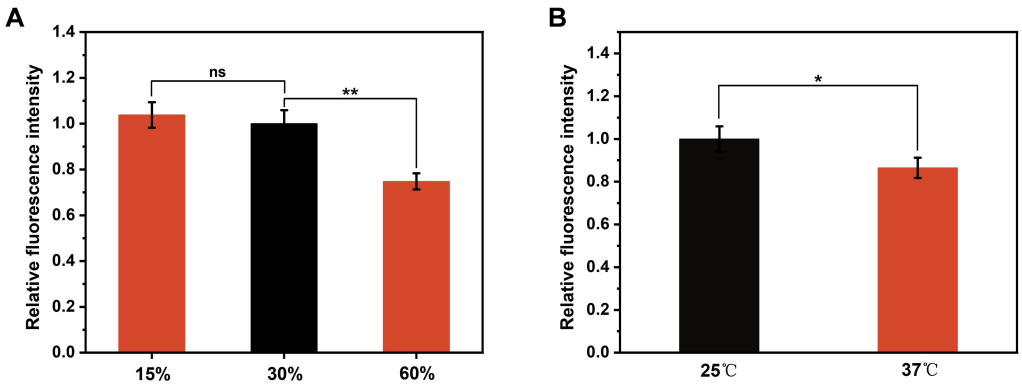

Figure S2. Stability of RhB in PMMA/HA-MNs under different environmental conditions. (A) Relative fluorescence intensity of RhB in PMMA/HA-MN stored at 25 °C under different humidity levels. (B) Relative fluorescence intensity of RhB in PMMA/HA-MN stored at 30% humidity under different temperatures. *P < 0.05, **P < 0.01, ns: no significance.

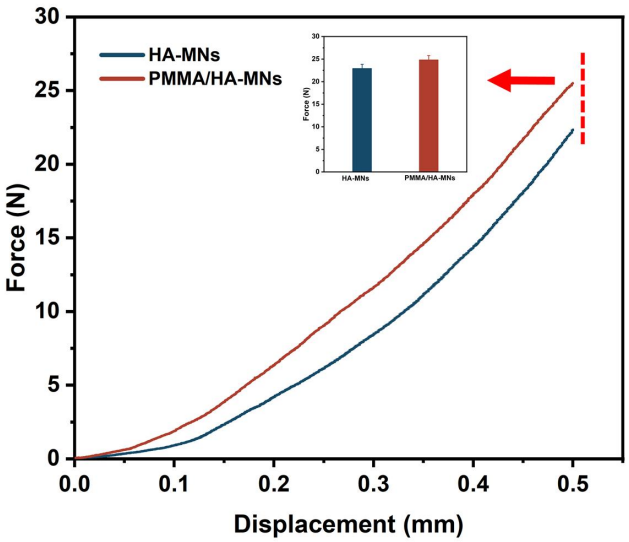

Figure S3. Force-displacement curves of PMMA/HA-MNs and HA-MNs.

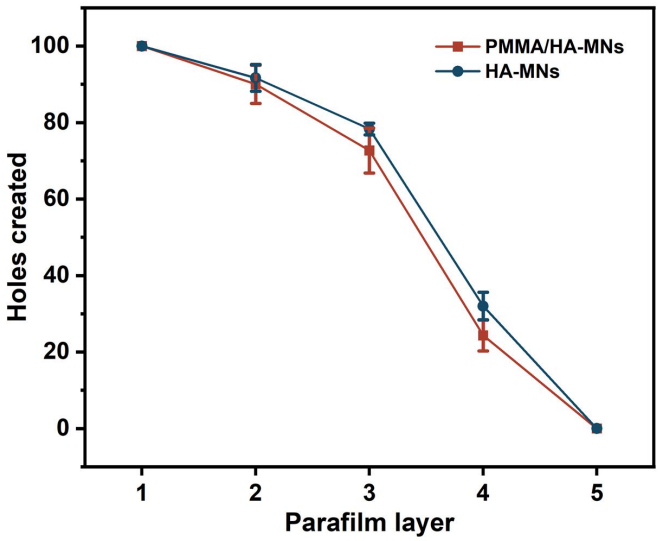

Figure S4. Number of holes created by PMMA/HA-MNs and HA-MNs on each layer of parafilm.

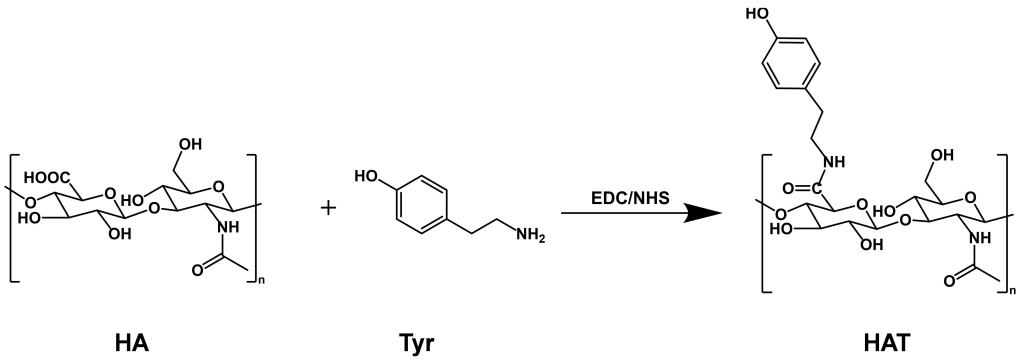

Figure S5. Schematic diagram of the HAT synthesis route.

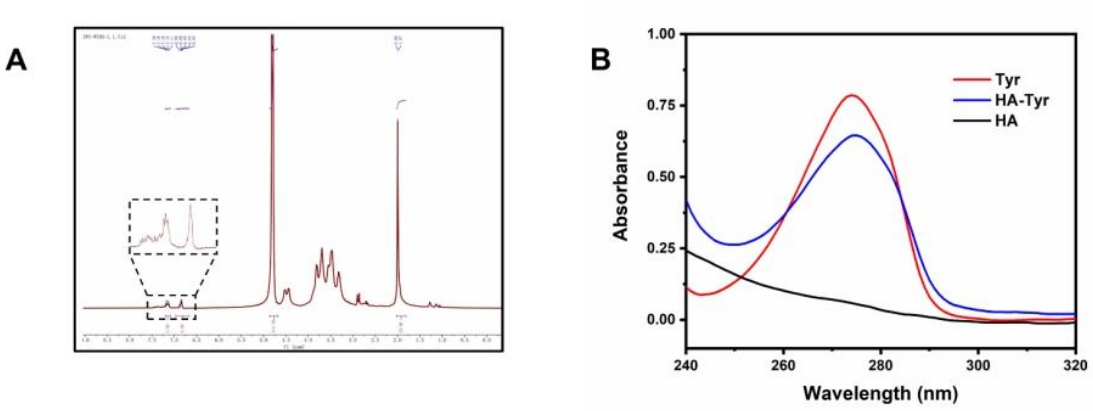

Figure S6. Characterizations of HAT. (A) ^{1}H NMR spectrum of HAT. (B) UV absorption spectrum of HAT.

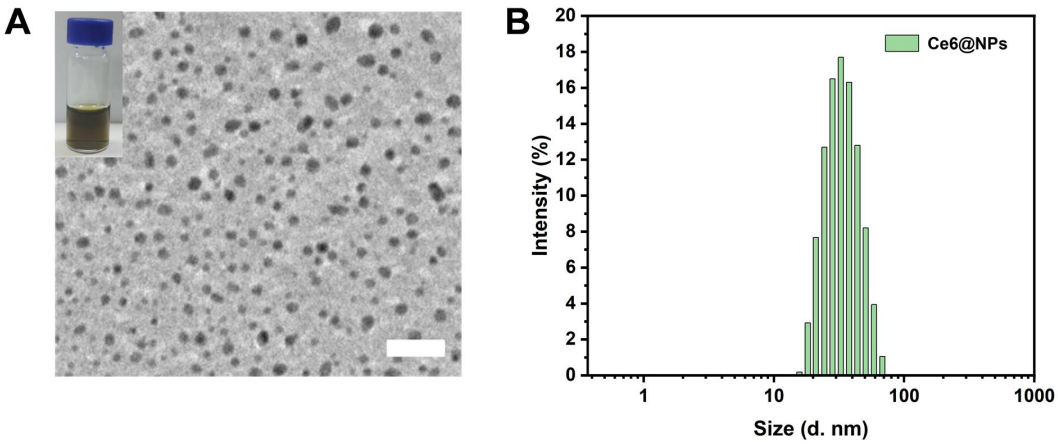

Figure S7. Morphological characterizations of Ce6@NPs. (A) TEM micrograph, inset shows the optical image of Ce6@NPs. Scale bar, 50 nm. (B) Size distribution.

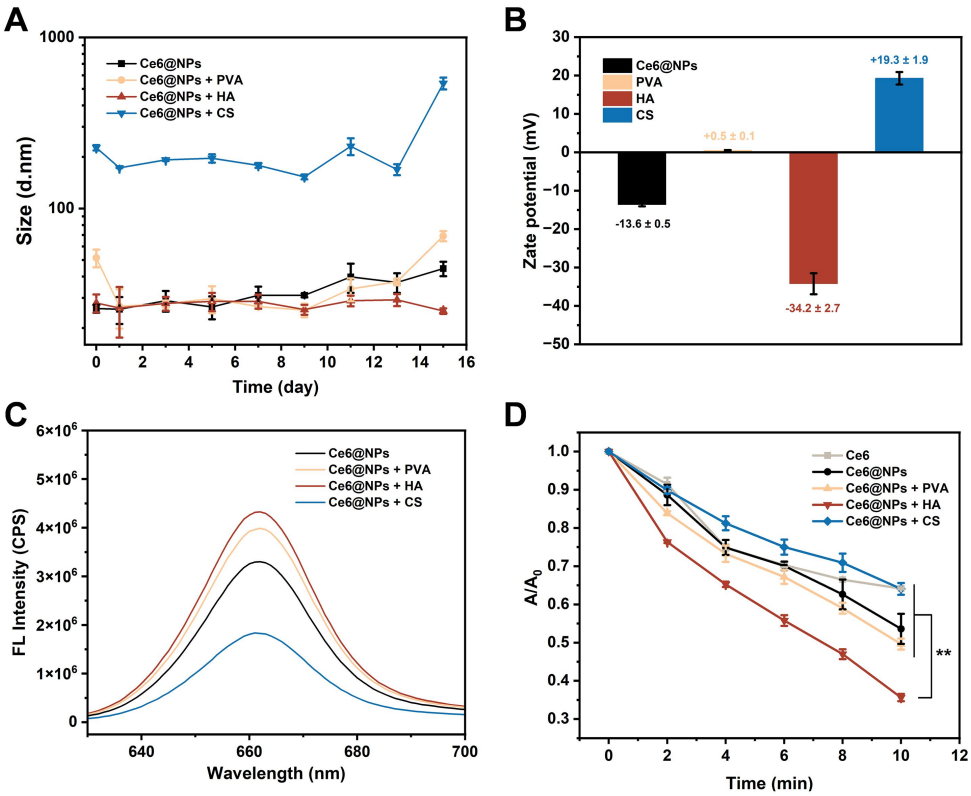

Figure S8. Effects of various matrix materials on the properties of Ce6@NPs. (A) Particle size of Ce6@NPs dispersed in various matrix materials. (B) Zeta potential of Ce6@NPs. (C) Fluorescence intensity of Ce6@NPs. (D) Absorbance changes of ABDA after Ce6 and Ce6@NPs received laser irradiation. **P < 0.01.

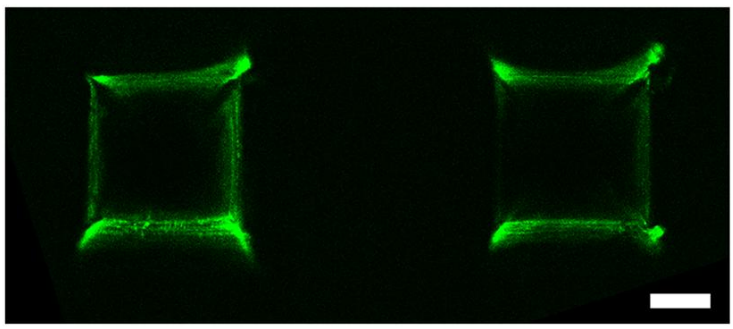

Figure S9. Representative images of the core-shell structured PCHAT-Ce6@NPs-MNs. FITC-labeled PCHAT shell (green). Scale bar: 100 μm.

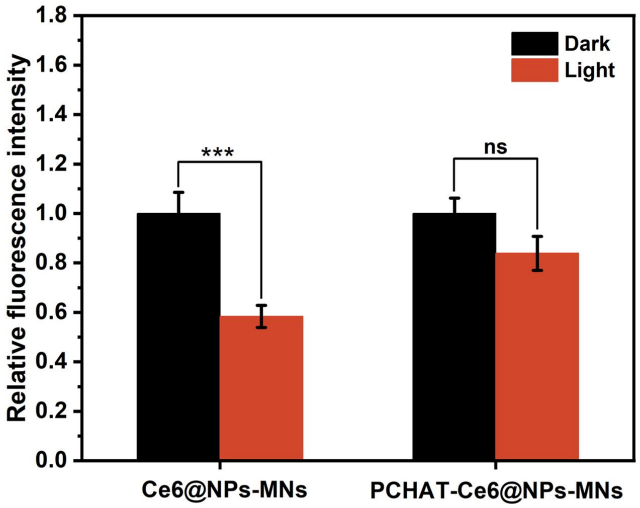

Figure S10. Relative fluorescence changes of Ce6 in Ce6@NPs-MNs and PCHAT-Ce6@NPs-MNs under blue light irradiation. ***P < 0.001; ns: no significance.

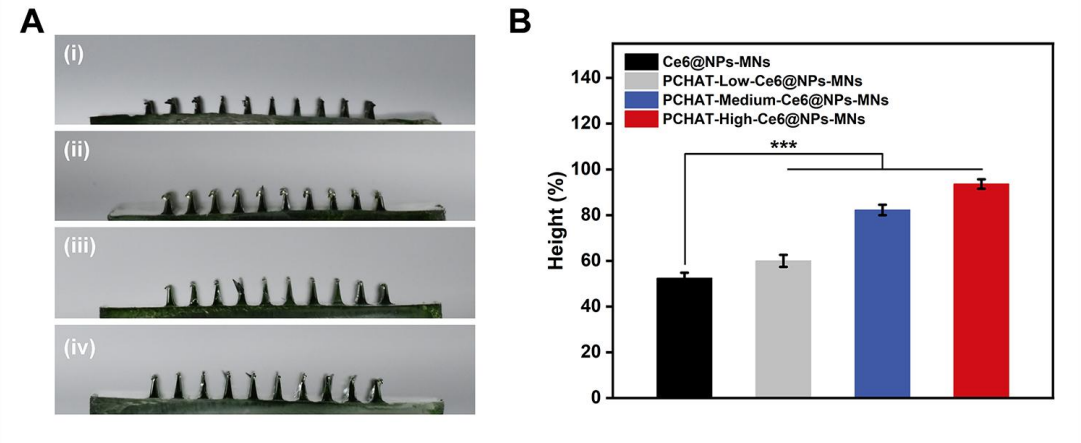

Figure S11. (A) The images of PCHAT-Ce6@NPs-MNs after application of a 30 N mechanical force. (i) Ce6@NPs-MNs, (ii) PCHAT-Low-Ce6@NPs-MNs, (iii) PCHAT-Medium-Ce6@NPs-MNs and (iv) PCHAT-High-Ce6@NPs-MNs. (B) The percentage of height of four MNs. ***P < 0.001.

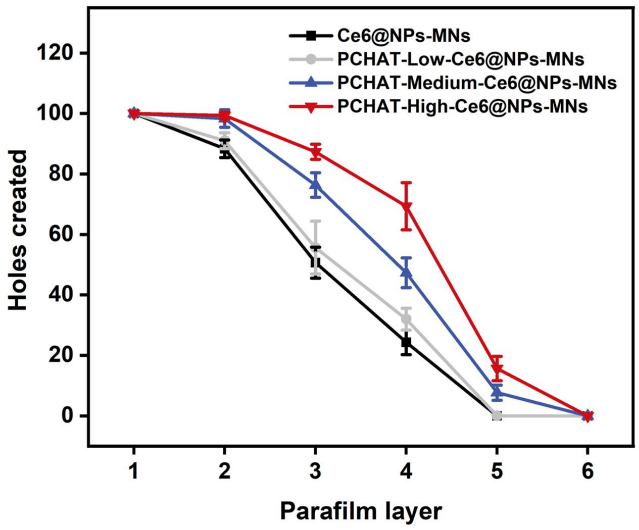

Figure S12. Number of holes created by Ce6@NPs-MNs and various PCHAT-Ce6@NPs-MNs on each layer of parafilm.

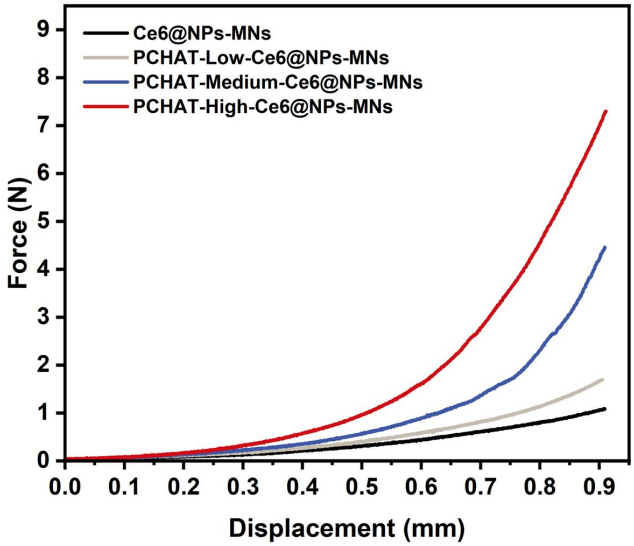

Figure S13. The puncture force-displacement curves of various microneedles on porcine skin.

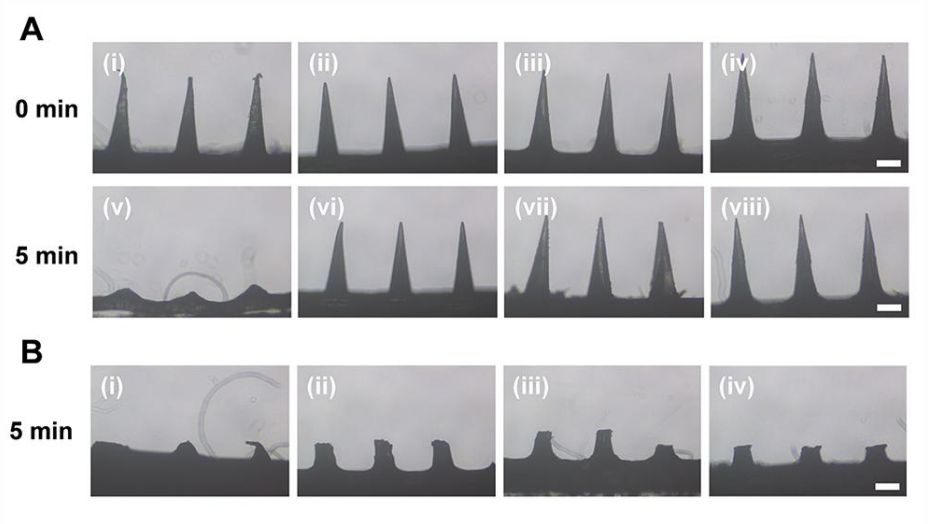

Figure S14. (A) Optical microscopy images of four MNs after insertion into agarose gel at different time points. (i) Ce6@NPs-MNs, (ii) PCHAT-Low-Ce6@NPs-MNs, (iii) PCHAT-Medium-Ce6@NPs-MNs and (iv) PCHAT-High-Ce6@NPs-MNs. (B) Optical microscopy images of four MNs after insertion into porcine skin after 5 min. (i) Ce6@NPs-MNs, (ii) PCHAT-Low-Ce6@NPs-MNs, (iii) PCHAT-Medium-Ce6@NPs-MNs and (iv) PCHAT-High-Ce6@NPs-MNs. Scale bar: 200 μm.

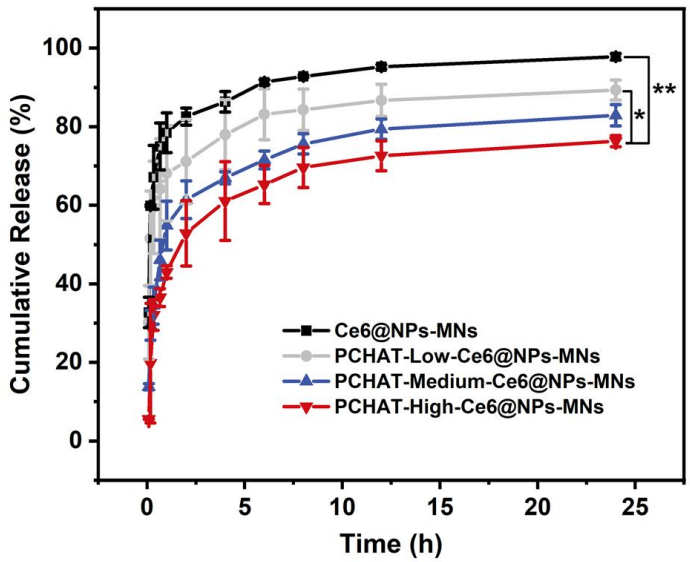

Figure S15. Percentage of drug release from Ce6@NPs-MNs, PCHAT-Low-Ce6@NPs-MNs, PCHAT-Medium-Ce6@NPs-MNs and PCHAT-High-Ce6@NPs-MNs at different time points. *P < 0.05; **P < 0.01.

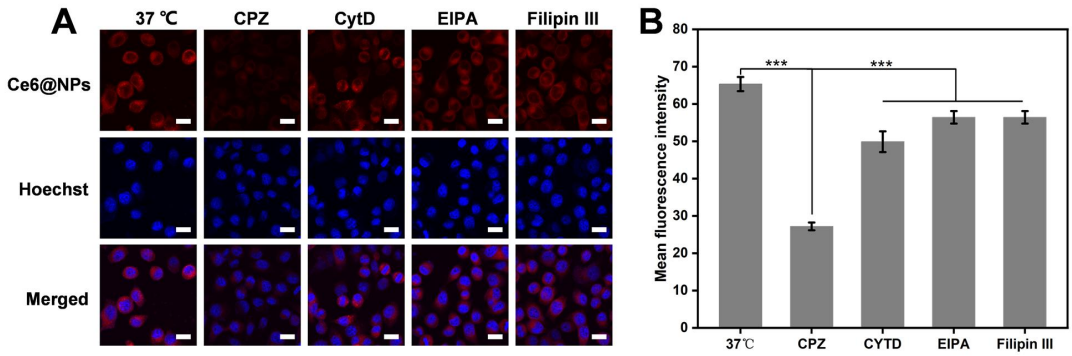

Figure S16. (A) CLSM images of A375 cells receiving 2 h pretreatment of 30 μM CPZ, 1 μg/mL Filipin III, EIPA 50 μM or CytD 20 μM prior to the addition of Ce6@NPs + HA. Scale bar: 20 μm. (B) The mean fluorescence intensity of red signals in the cells images of (A). ***P < 0.001.

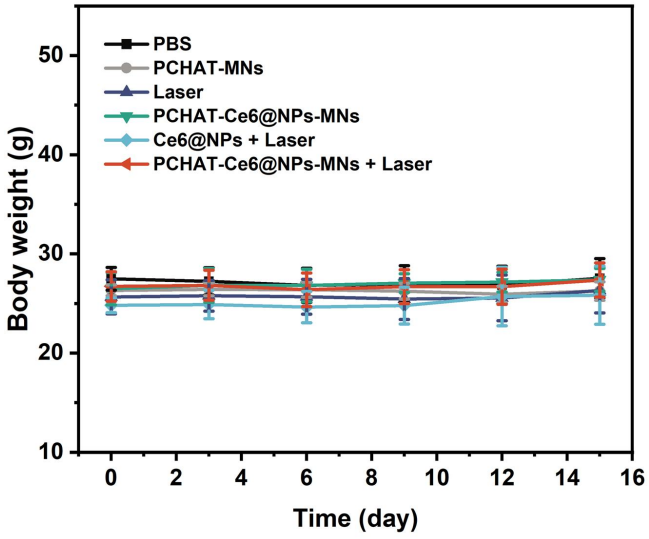

Figure S17. Changes of body weight in A375-xenografted mice after various treatments.

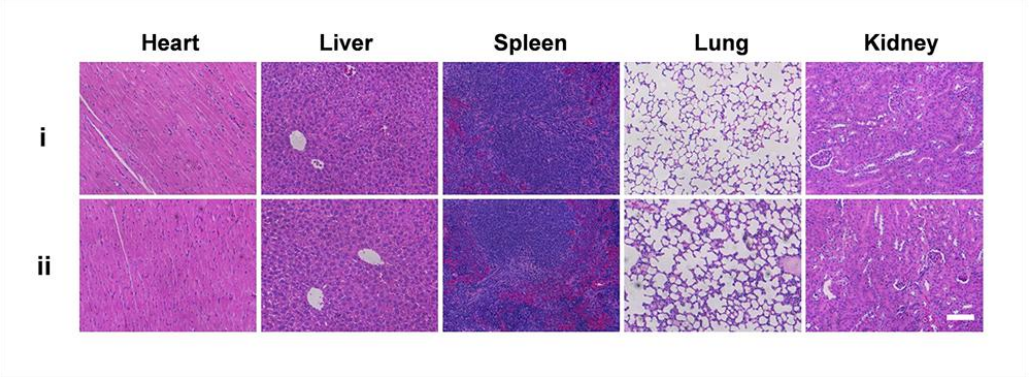

Figure S18. Representative H & E-stained images of major organ tissues (heart, liver, spleen, lung, kidney) from mice after different treatments. Groups: (i) PBS; (ii) PCHAT-Ce6@NPs-MNs + Laser. Scale bar: 100 μm.

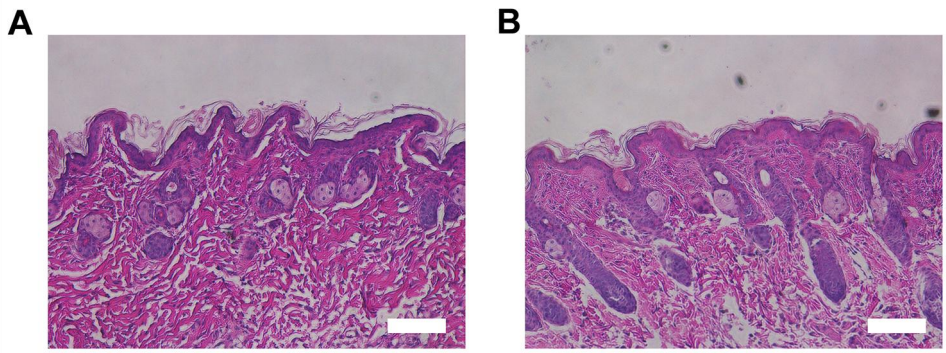

Figure S19. Histological analyses of skin tissue at the laser sites. (A) H & E staining of skin tissue before laser irradiation. (B) H & E staining of skin tissue after 5 min of laser irradiation. Scale bar, 500 μm.

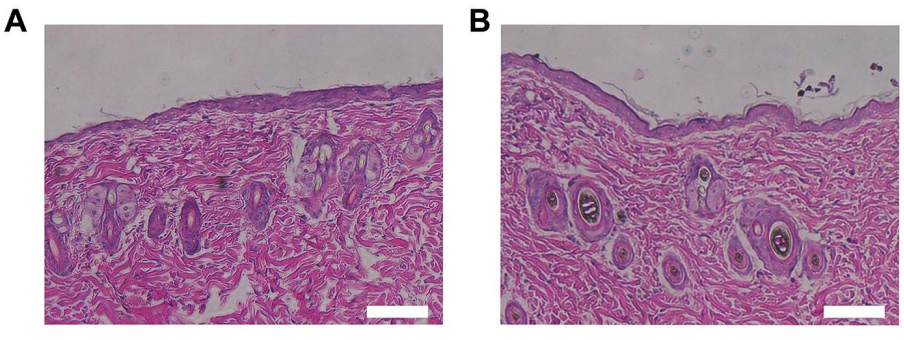

Figure S20. Histological analysis of skin tissue at the site of microneedle application. (A) H & E staining of skin tissue from the control group. (B) H & E staining of skin tissue 15 days after microneedle application. Scale bar: 500 μm.

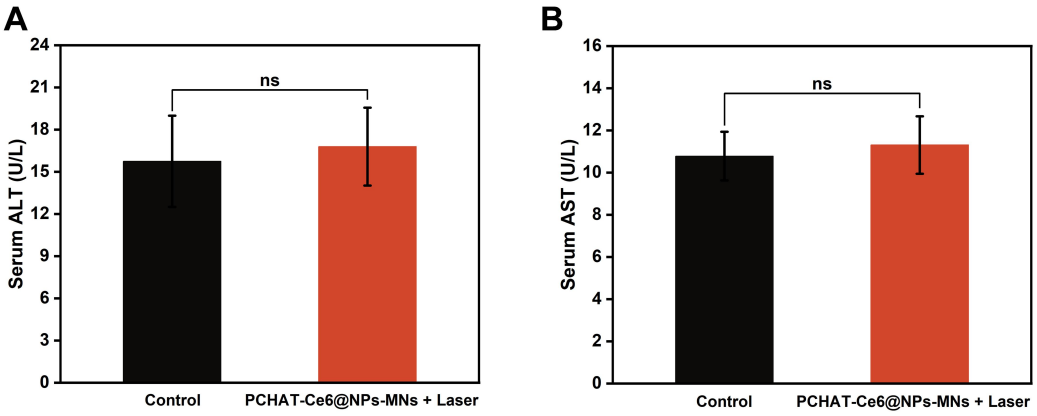

Figure S21. Quantitative analysis of serum ALT (A) and AST (B) levels after 15 days of different treatments. ns: no significance.

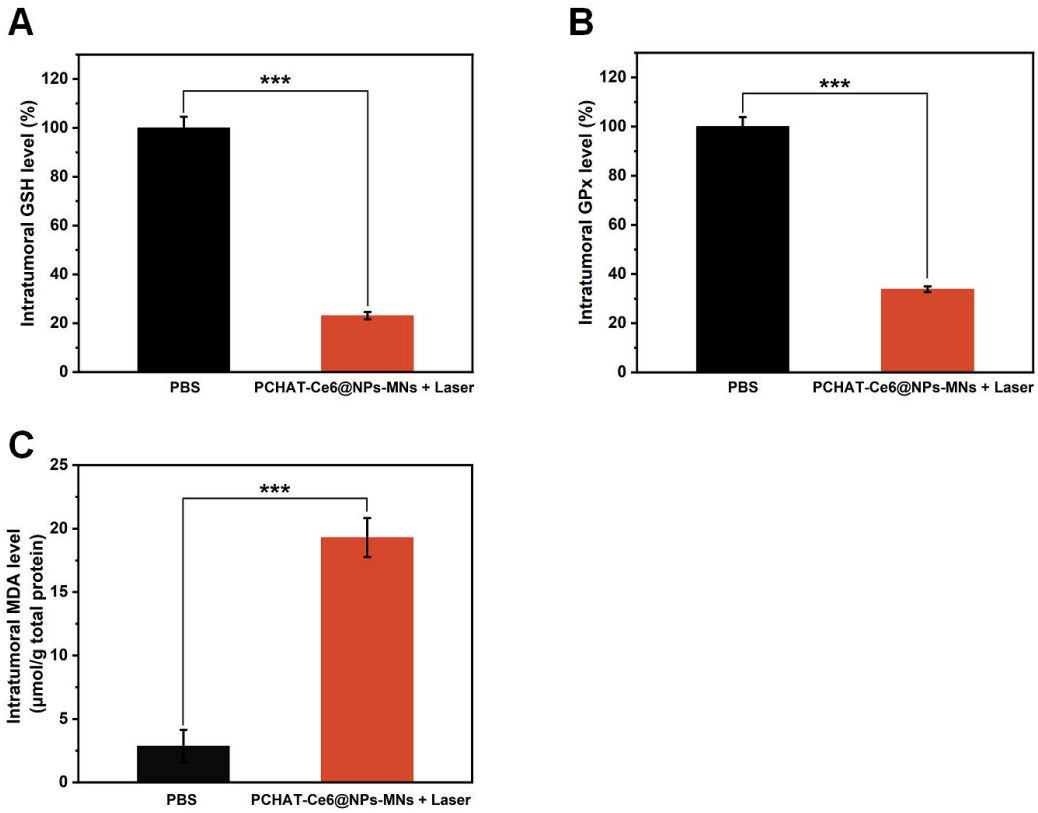

Figure S22. Quantifications of GSH (A), GPx (B), and MDA (C) levels in tumor tissues after various treatment. ***P < 0.001.

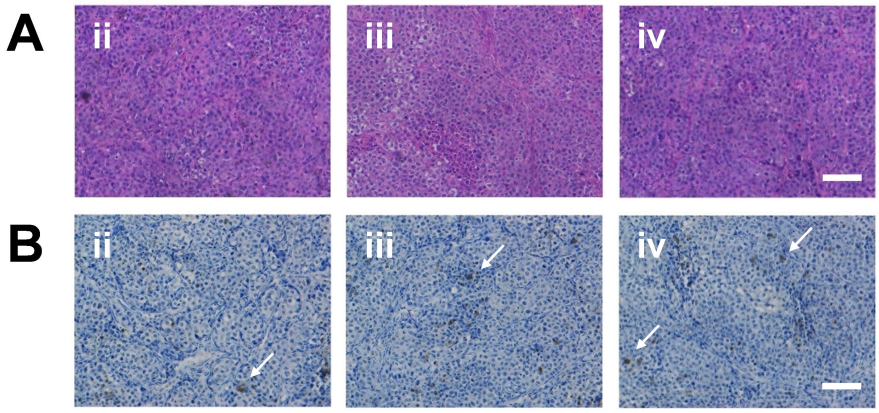

Figure S23. (A) Representative H & E-stained images of tumor tissue sections after various treatments. (B) Representative TUNEL-stained images of tumor tissue sections, with arrows indicating apoptotic cells. Groups: (ii) PCHAT-MNs; (iii) Laser; (iv) PCHAT-Ce6@NPs-MNs. Scale bar: 100 μm.

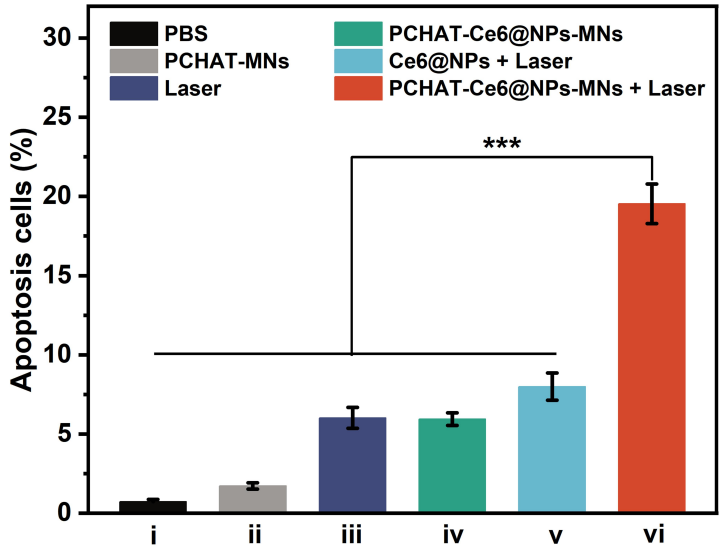

Figure S24. Percentages of apoptotic cells in tumor tissues after various treatment. ***P < 0.001.

Reference

1 Zhao, J. Li, Y. Su, L. Yang, L. Chen, L. Qiang, Y. Wang, H. Xiang, H. Tham, J. Peng and Y. Zhao, MTH1 inhibitor amplifies the lethality of reactive oxygen species to tumor in photodynamic therapy, *Sci. Adv.*, 2020, **6**, eaaz0575.